40th Fluid Dynamics Conference and Exhibit
28 June - 1 July 2010, Chicago, Illinois

AIAA 2010-4475

Characteristics of a turbulent boundary layer perturbed by spatially-impulsive dynamic roughness

I. Jacobi, M. Guala & B. J. McKeon*

Statistical and spectral analyses of the manipulation of a canonical zero pressure gradient turbulent boundary layer using static roughness and low-frequency dynamic roughness patches are presented. A shift of spectral energy away from the wall downstream of the roughness patch is observed. The dynamic roughness is shown to disrupt the structure of the boundary layer, while embedding its periodic signature in an extensive stretch of the downstream flow field.

I. Background

Zero-pressure gradient turbulent boundary layer flow over a flat plate has been studied extensively and significant progress has been made towards a conceptual understanding of the structure and evolution of turbulence. Near the wall, a process of ejections and sweeps of fluid, often described as a bursting phenomenon, is thought to contribute significantly to the production of turbulence. These ejection and sweep motions constitute a near-wall cycle of fluid motions which have a controlling influence on the Reynolds stress near the wall and are closely associated with vortex structures located throughout the wall region[1,2] Much of this same general framework applies equally to the case of a uniformly rough flat plate, however roughness is thought to alter the mechanics of fluid entrainment and ejection at the wall – producing a more violent entrainment and nearly vertical ejection due to roughness geometry. Thus, the rough wall condition permanently disturbs the buffer layer viscous cycle of the corresponding smooth wall.[3] Both of these well-studied flow situations present an equilibrium turbulent boundary layer, where the flow can be described entirely in terms of local turbulent processes. The less studied problem of non-equilibrium boundary layers, which depend on non-local factors, is acutely interesting because of the insight it potentially offers into the dynamic processes of the evolution of turbulent structure. In addition, these non-equilibrium situations are of significant practical interest,[4] with relevance to pipes, wings, or other flow surfaces over which surface roughness and other properties change passively, and also in which control systems are designed to actively perturb flows.

Flow over a surface which transitions between a rough and smooth boundary condition offers the simplest case for non-equilibrium behavior downstream of transition. For the transition from a smooth to rough surface, studied by Antonia and Luxton,[5] the return to equilibrium was observed by the development of an internal layer which was born at the transition point and grew quickly to the edge of the boundary layer itself, thereby re-establishing equilibrium within twenty boundary-layer thicknesses. The transition from a rough to smooth wall condition showed significantly slower growth of the corresponding internal layer and experimentally the restoration of equilibrium was never observed.[6] Subsequently, the problem of a spatial impulse of roughness on an otherwise smooth boundary was considered by Andreopoulos and Wood,[7] since it provided an opportunity to isolate the influence of the roughness in a patch short enough to avoid establishment of equilibrium. In this way, the additional length scale of the roughness was introduced to the turbulent boundary layer and the response of the boundary layer could be observed downstream independent of the continued presence of the roughness itself. The growth of both internal layers, one from each boundary transition, was observed to be consistent with their independent growth rates, and the overall recovery was dominated by the rough to smooth transition.

*Graduate Aerospace Laboratories, California Institute of Technology, Pasadena, CA 91125, U.S.A.

The present study introduces both a roughness length scale and a time scale, by dynamically actuating a spatial impulse of roughness at a fixed frequency, so that the boundary condition alternates between smooth and impulsively rough. This dynamic perturbation is compared to the static roughness impulse of equivalent dimension.

II. Experimental Method

Experiments were performed in the $2' \times 2'$ wind tunnel at Caltech in a zero pressure gradient turbulent boundary layer. The test section of the tunnel had an rms spatial variation in pressure coefficient, $\Delta C_p \ll 0.01$. A spatial impulse disturbance of two-dimensional, k-type roughness was introduced at a streamwise position corresponding to a local Reynolds number based on momentum thickness, $Re_\theta = 2700$. Two dimensional roughness provides larger ejection events, and thus a larger impulsive effect on the flow, than three-dimensional elements,[8] and also forces all spanwise planes to behave similarly. The time-periodic roughness amplitude was generated using a two-dimensional roughness pattern which fit into channels carved into the test plate such that the roughness elements could move freely through the plate (figure 1), while at the same time allowing no through-flow between the upper and lower surfaces of the plate.

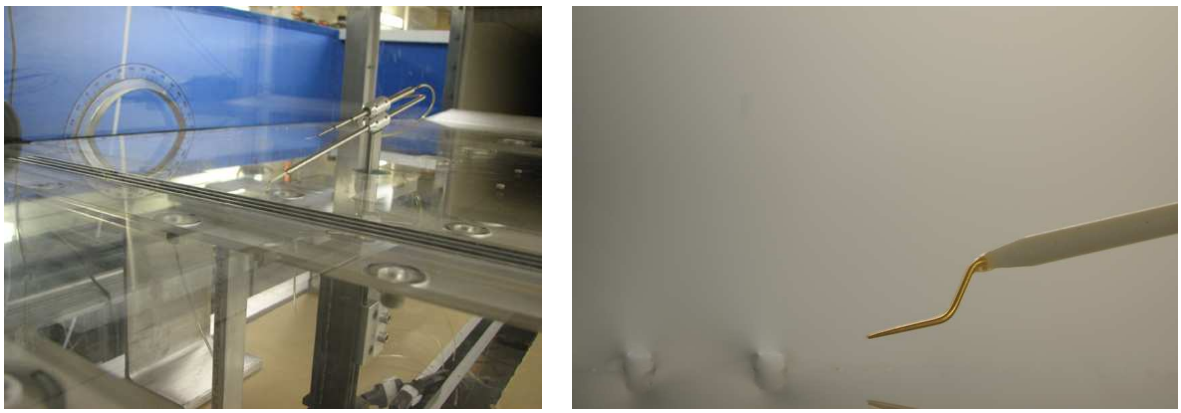

Figure 1. (Left) The roughness array installed along the flat plate – the hotwire and its traverse are visible in the background; (Right) The probe just downstream of the individual roughness elements at full extension, $1050 \pm 40\mu m$

Details of the roughness elements were provided previously[9] but to reiterate briefly: the elements are configured to provide an interstitial distance to height ratio of 6.35, to maximize the roughness-type behavior[10] and the total streamwise extent of the roughness elements is approximately one and a half boundary layer thicknesses, such that it fulfills the spatially impulsive requirement.[7] The roughness was driven by a reciprocating D/C motor positioned beneath the test section of the wind tunnel to achieve an order $k = 1$ mm amplitude motion, which corresponds to $k/\delta = 0.06$ or, in inner units with reference to the smooth wall friction velocity, $k^+ \equiv ku_\tau/\nu \approx 55$.

The velocity field was explored by hot-wire anemometry, recording time-series of the longitudinal velocity at 27 logarithmically spaced heights and 10 logarithmically spaced streamwise locations downstream of the roughness patch (60 kHz, 3×10^6 points per wall normal location), for both a static roughness with height identical to the maximum amplitude of the dynamic case, and the dynamically actuated case itself. The results are normalized, in outer units, according to the recorded boundary layer thickness (δ_{99}) in each regime (figure 2) and the free stream velocity, $U = 20.1$ m/s (which was fixed in all three regimes to within measurement error, ± 0.1 m/s); for inner units, all normalizations are in reference to the smooth wall friction velocity, which means that $\delta^+ \approx 900$.

III. Statistical Results

The first question addressed was the relaxation of the flow field downstream of the roughness. Both the mean velocity profile (figure 3) and the turbulent statistical profiles (figure 4) for static and dynamic roughness

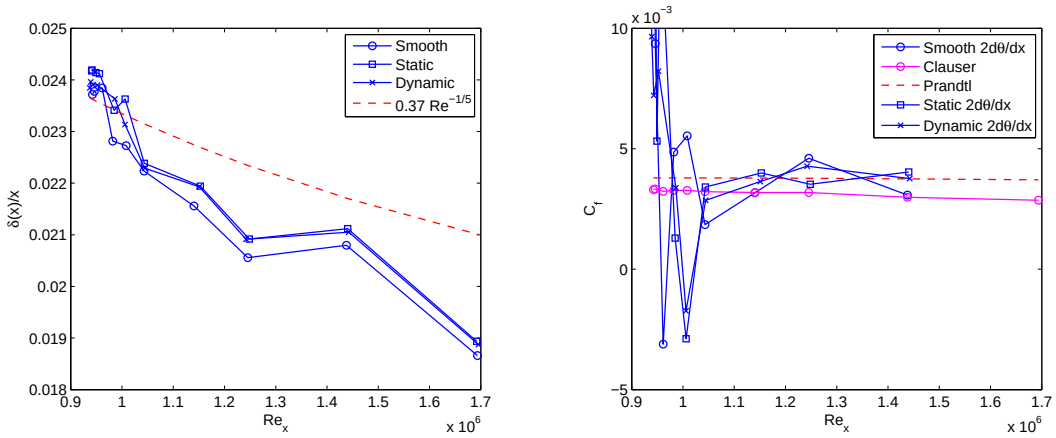

Figure 2. (Left) The development of the boundary layer thickness (δ_{99}), for the different test scenarios, along with the quasi-empirical fit from Prandtl; (Right) The development of the skin-friction coefficient, as determined by the Clauser method and also by the momentum integral approach; for the perturbed cases, the momentum integral approach is not strictly valid due to the non-equilibrium

appeared to converge to the smooth wall profiles within 10 δ of the perturbation (consistent with previously reported preliminary measurements[9]). However, measurements of the internal layers (figure 5) demonstrate their presence very far downstream, suggesting a continued structural influence of the impulse even far downstream,[7] at distances of $x/\delta > 25$.

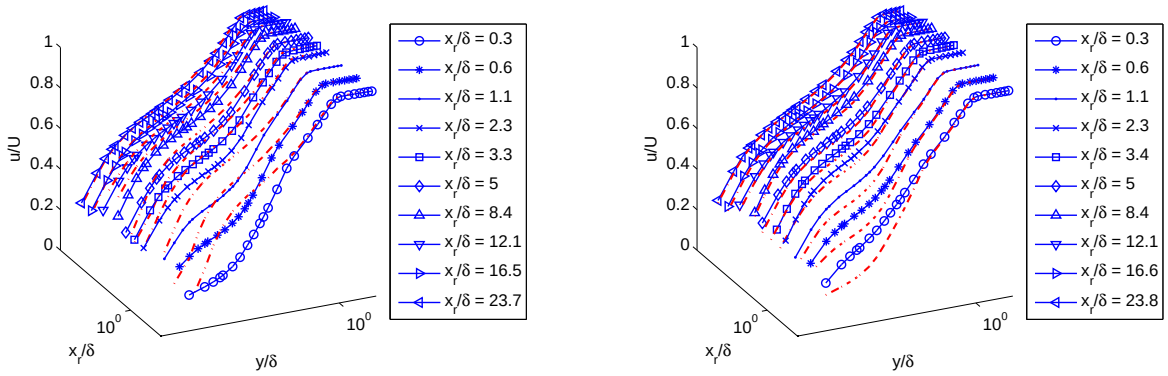

Figure 3. (Left) The mean velocity profile, in outer units, for the static perturbation. The dotted line is the velocity profile from the smooth wall, at the identical physical location.(Right) The mean velocity profile, in outer units, for the dynamic perturbation. The dotted line is the velocity profile from the static perturbation, for comparison, at the identical physical location.

From the plots above, it is clear there is a qualitative distinction between the static and dynamic perturbations. Statistically, both roughness conditions produce a 'hump' in turbulence intensity profile, indicative of increased mixing farther from the wall. The dynamic perturbation produced a broader 'hump', showing increased turbulence intensity at all heights below the usual peak for a rough wall.[9] In order to compare all of the profiles, contour plots were constructed based on the deviation of the static and dynamically-perturbed profiles from the smooth flow turbulence profile according to equation (1) (figure 6), with each term normalized in outer units. The non-equilibrium flow downstream of the perturbation means that standard techniques for estimating u_τ by either Clauser's method or the Karman momentum integral are not strictly valid, and thus inner normalizations are not straightforward; as noted above, where necessary, the value of u_τ from the unperturbed flow (smooth wall) is employed.

$$\Delta\overline{u'^2}(x,y) = \overline{u'^2}(x,y)_{perturbed} - \overline{u'^2}(x,y)_{smooth} \tag{1}$$

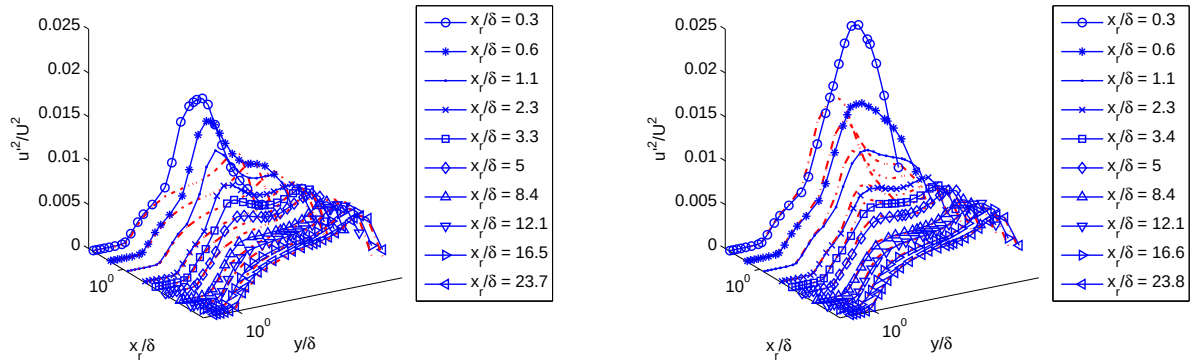

Figure 4. (Left) The turbulence intensity profile, in outer units, for the static perturbation. The dotted line is the velocity profile from the smooth wall, at the identical physical location.(Right) The turbulence intensity profile, in outer units, for the dynamic perturbation. The dotted line is the velocity profile from the static perturbation, at the identical physical location. Note the wider 'hump' associated with the dynamic perturbation. Also note the direction of axes, which are arranged in order not to obscure the relaxation trend

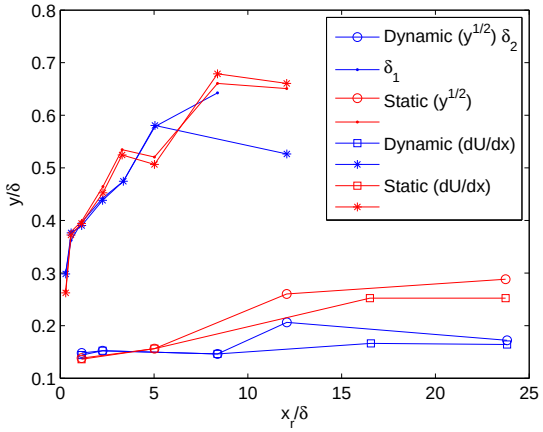

Figure 5. The internal layer boundaries, as inferred by using a $y^{1/2}$-scaling,[11] and also by successive streamwise derivatives of the velocity profile, dU/dx, which produce self-consistent results, despite the slight subjectivity inherent in each method independently; δ_1 represents the internal layer from the smooth to rough transition and δ_2 the rough to smooth transition, at the trailing edge of the impulse

Immediately it is clear that the static perturbation produces a large mean velocity deficit; the dynamic perturbation mitigates this deficit somewhat, both in intensity and in streamwise extent. If we consider the rms roughness height $k_{rms} = k_{static}/\sqrt{2}$ for the sinusoidally-driven dynamic perturbation, then the ratio of k_{static}/k_{rms} explains a significant portion (60-70%) of the variation in the mean velocity defect. For the turbulence intensity, $\overline{u'^2}$, that mitigation of the effect of the statically-perturbed flow is reversed – the dynamic perturbation tends to significantly increase the turbulence intensity, notably even near the wall, at smaller wall normal locations than the static perturbation effects; although, in the near wall region, the relative spatial impact of dynamic roughness is quite localized. The additional 'hump' seen in the static and dynamic turbulence intensity profiles now can be clearly seen to move outward as it dissipates going downstream.

IV. Spectral Results

The anemometer signals were processed using Welch's method to generate pre-multiplied energy spectra for the streamwise velocity component u such that a map of the spectral energy distribution (composite

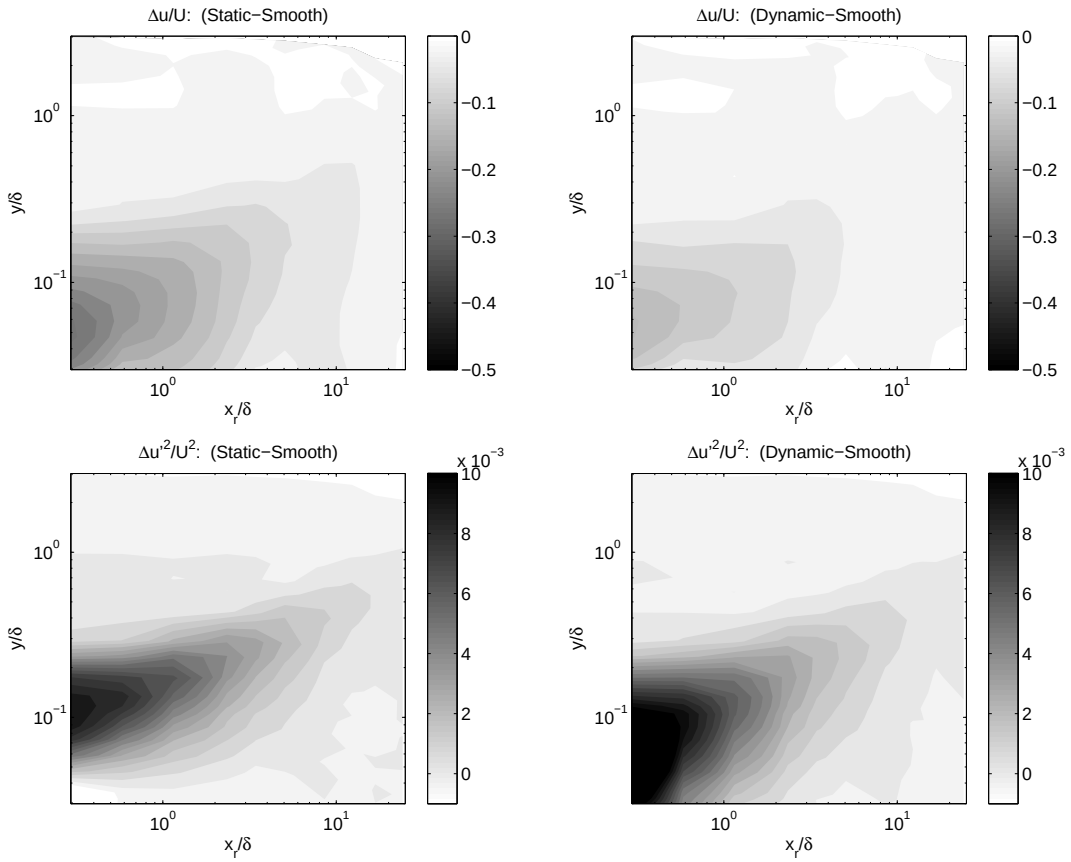

Figure 6. (Top) The mean velocity variation contours: left is the statically-perturbed minus smooth case,right is the dynamically-perturbed minus smooth (Bottom) The turbulence intensity variation $\Delta\overline{u'^2}(x, y)$ contours: left and right normalized as on top

spectrum) would represent equal energetic content via equal areas (figures 8 and 9). Taylor's hypothesis, using the local mean velocity, was employed in order to transform the temporal spectra into spatial spectra.

In the first streamwise location downstream of the roughness (but outside the recirculation bubble), the spectral energy associated with the near wall peak appears to have been displaced in both the static and dynamic cases, while in addition, it appears to have broadened in wavelength-space. The broadening is more prominent for the static then the dynamic case, although the dynamic case shows very distinctive harmonics of the perturbation which appear to extend throughout the boundary layer. By the next streamwise position, the near wall peak appears to be recovering in both cases, and this recovery appears to proceed until at least 16δ downstream of the original perturbation, but even here, where the composite spectrum looks very close to the corresponding smooth wall spectrum (figure 7), nevertheless the dynamically perturbed case still shows a prominent signature of the periodic perturbation.

The broader peak in the static case is biased towards longer wavelengths farther from the wall (and to a lesser extent shorter wavelengths nearer to the wall). This bias is most obvious at the location $x/\delta = 0.6$ (figure 8). Specifically, the bias extends from normalized wavelengths of 8 to 15 δ; see the Discussion section on page 6.

A three-dimensional map of the composite spectra recorded at 10 streamwise locations can be constructed in order to highlight the evolution of the most intensely energetic content (figure 10). The initial diminution of the near wall spectral content, along with the apparent displacement of spectral energy away from the wall, is seen to evolve downstream to the familiar shape of the near wall peak from the smooth wall case. Although even at 25δ downstream, there is still a consistent appearance of the dynamic signature, despite the observation earlier that the energetic 'hump' of the $\overline{u'^2}$ associated with the roughness had completely passed through the boundary layer by that point.

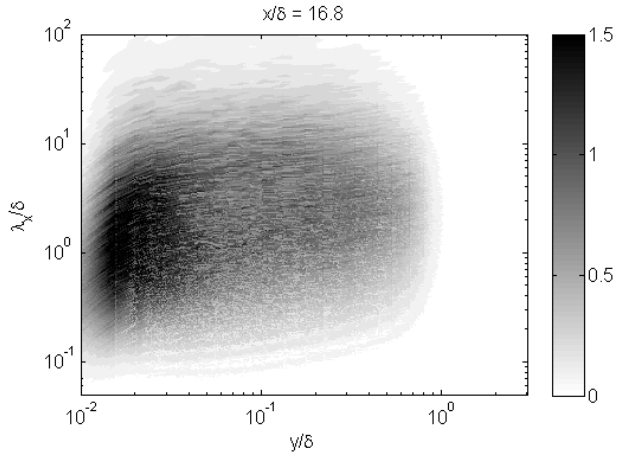

Figure 7. The smooth wall composite spectrum, at the physical location corresponding to the dynamic spectrum at $x/\delta \approx 16$ for convergence comparison; also the levels of the contour plot, representing the pre-multiplied energy spectrum kP_{xx}/u_τ^2 are linear and range from dark (0) to light (1.5) and colors on all subsequent composite plots are identical

V. Discussion: Static versus Dynamic Perturbations

The presence of a broad energetic region, far from the wall, in the composite spectra for the static perturbation (and its narrower counterpart in the dynamic case) was identified previously. If we consider the possibility that this breadth (wider than the near-wall peak) is associated with shedding from the roughness elements either individually or as a group, an expected wavelength for the shedding can be estimated. Consider assuming that the roughness elements collectively shed vortices like half a cylinder extending from the flat plate. Then the Strouhal shedding frequency would be $St = fL/U = 0.2$, with overall streamwise extent of the roughness patch as $L = 0.025m$ and the convective velocity at the top of the elements $U = 11.4m/s$. Then the shedding frequency should be $\approx 100Hz$, which corresponds to a wavelength, using Taylor's hypothesis, of $\lambda = 0.125m$ or $\lambda/\delta \approx 8$, which is in the neighborhood of the observed bulge.

Extending this approach a bit: structures associated with shedding should be significantly smaller than those associated with the dynamic perturbation, since the frequency of the dynamic perturbation is $30Hz$; this can be seen clearly from the relative location of the harmonics of the dynamic perturbation in the dynamic composite spectra (figure 8). Also included in this lower-wavelength range are structures from the near wall upstream of the perturbation which were displaced and rearranged over the two-dimensional roughness elements. However, in order to get a more intuitive sense of the distribution of the energy associated with the different-sized structures and the way in which it changes downstream, the spectra can be integrated over bands of wavelengths. Since the spectra were originally normalized with the $\overline{(u'^2)}(x,y)$, equation (2), the previous contour plots (figure 6) can be recalculated, but including contributions to $\overline{(u'^2)}(x,y)$ from only distinct bands of wavelengths (figure 11).

$$\overline{u'^2}(x,y) = \int_{\lambda_x=0}^{\lambda_x=\infty} \Phi(\lambda_x', x, y)\, d\lambda_x' \tag{2}$$

A line has been fitted, by least-squares regression, to the peaks of the deviation, $\Delta\overline{u'^2}(x,y)$, of the perturbed $\overline{u'^2}(x,y)$ from that of the smooth wall. This line shows that a power-law relation describes the shift of the 'hump' associated with the perturbations, as the 'hump' shifts away from the wall and as it decreases in magnitude moving downstream. However, the rate at which this shift occurs is quite different between the static and dynamic perturbation (25% difference in the value of the exponent), despite visual appearances. The consequence of this difference is that the 'hump' associated with the static perturbation is expected, ignoring mixing and other effects downstream, to clear the boundary layer 75δ downstream of the impulse (extrapolating the power law to $y/\delta = 1$), whereas the 'hump' associated with the dynamic perturbation would clear the boundary layer in 50δ.

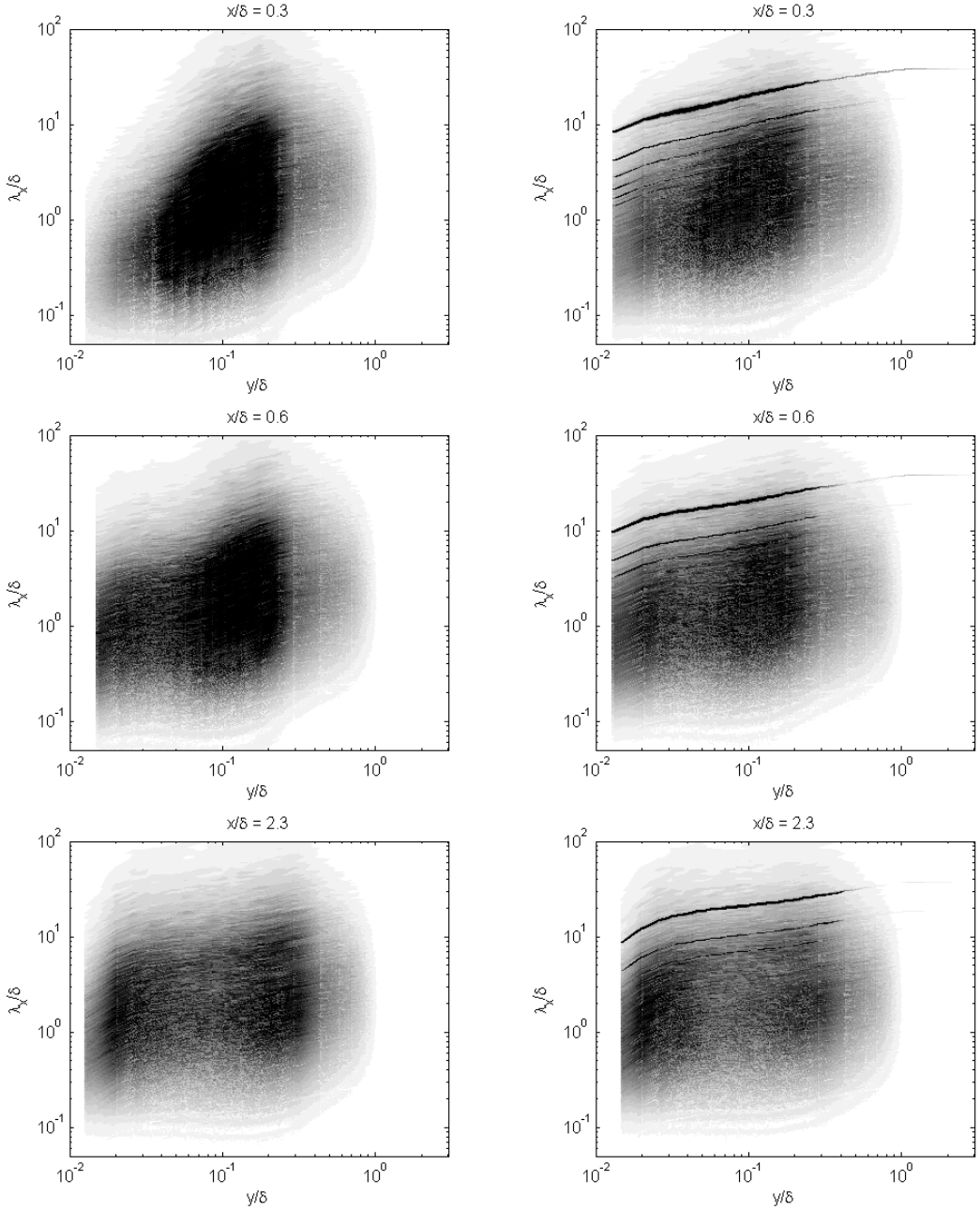

Figure 8. On the left are the spectra for the static perturbation regime; on the right those for the dynamic regime, at the corresponding streamwise locations.

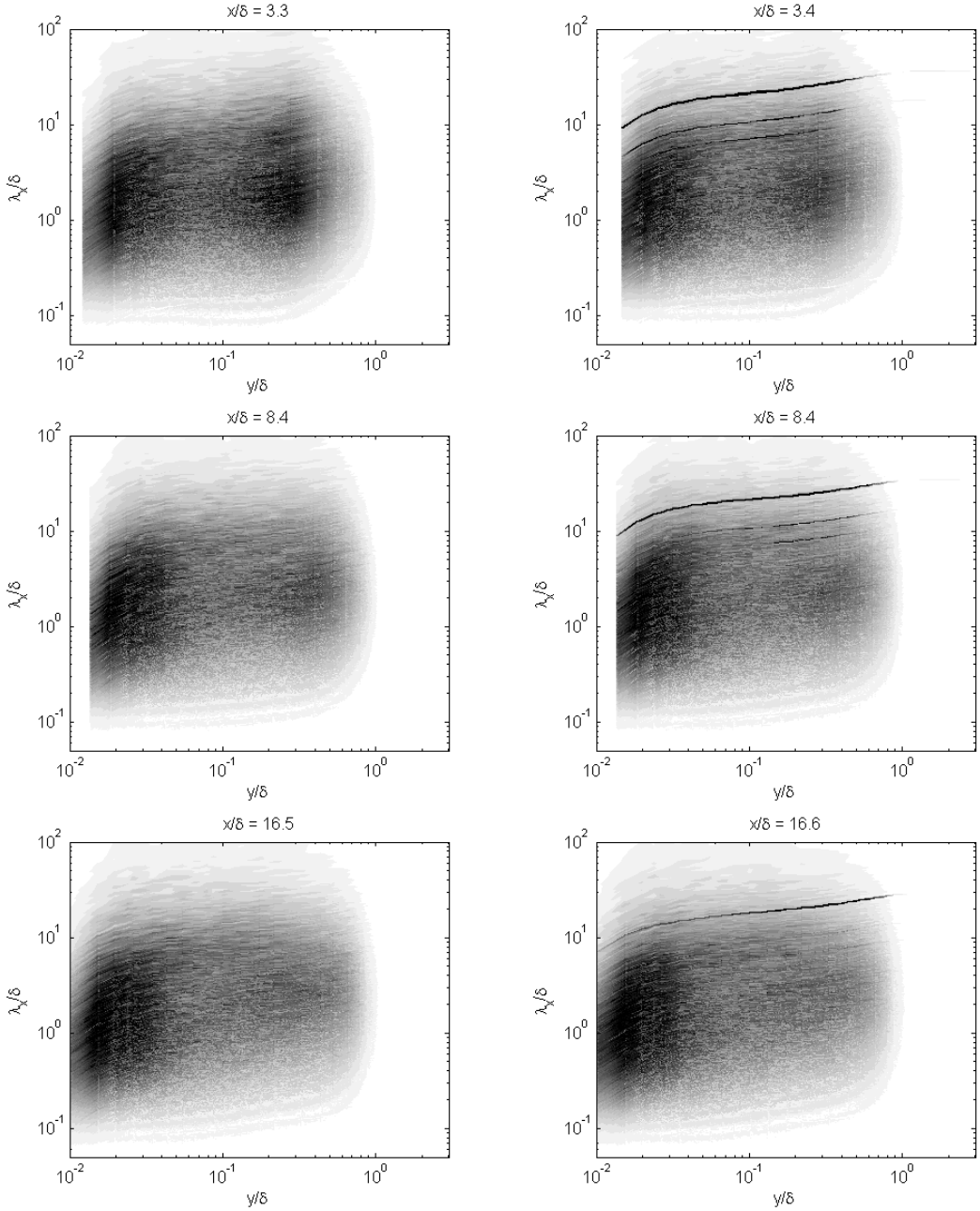

Figure 9. The spectra even further downstream from the roughness; as before, static on left and dynamic on right. Note that the signature of the temporal perturbation persists even far downstream

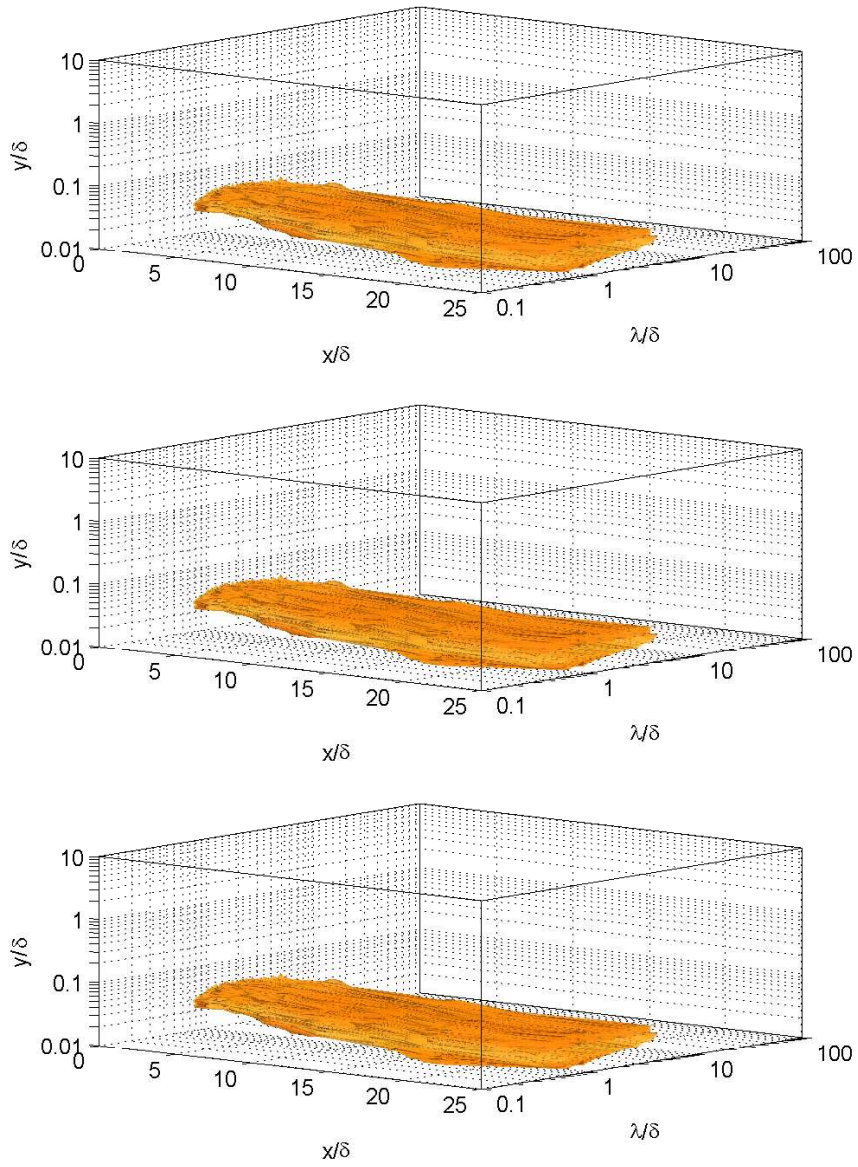

Figure 10. The individual composite spectra from each streamwise location (figures 8 and 9) are assembled into a three-dimensional representation; the surface contour encompasses all energy levels higher than 0.8 times the peak value from the smooth wall spectrum – which in the smooth wall case captures the bulk of the near wall-peak energy. Top is the smooth wall case, middle is the static roughness, and on bottom is the dynamic, showing the distinctive harmonics

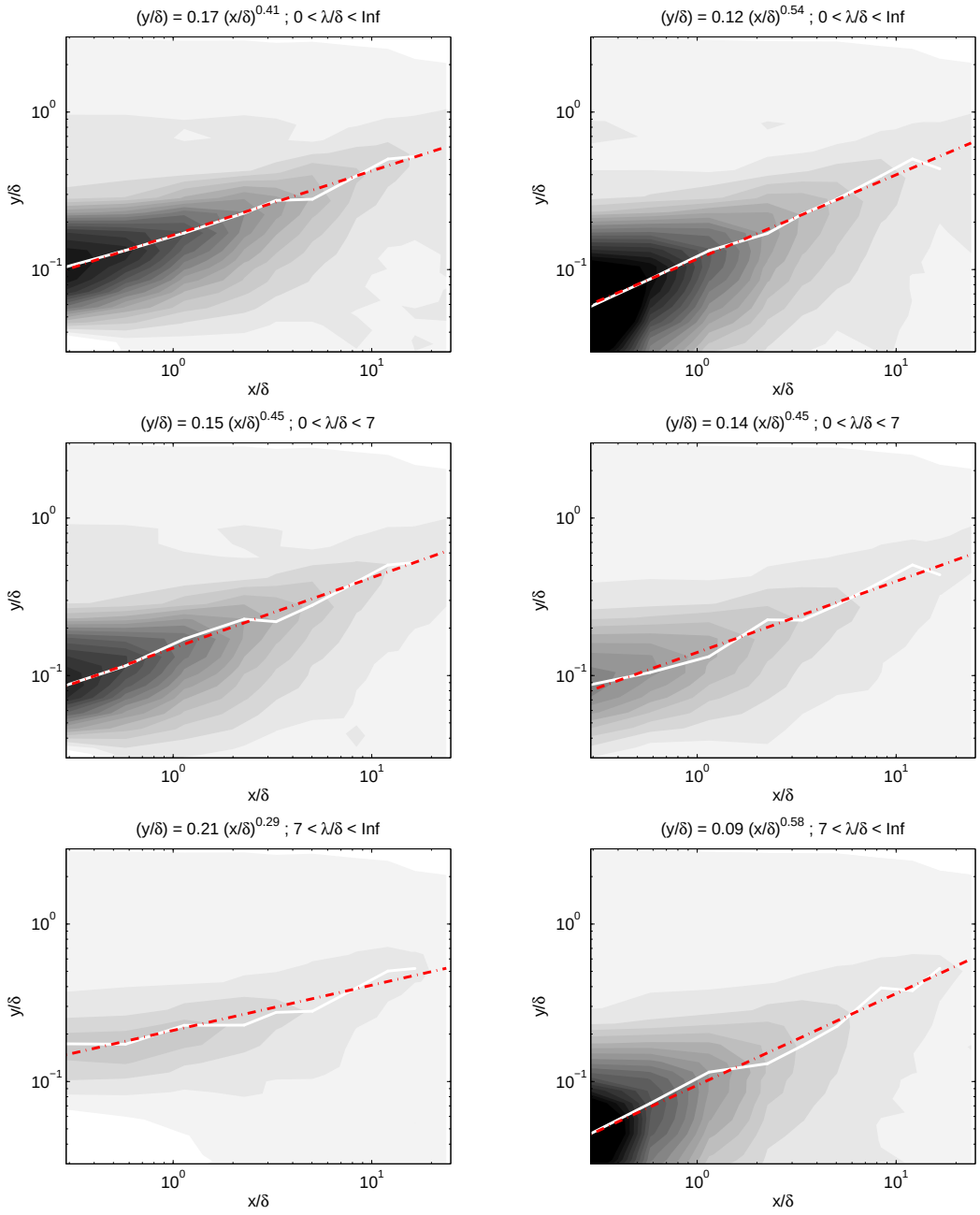

Figure 11. Recreating the turbulence intensity variation (figure 6) by integrating the streamwise wavelength spectra over different ranges of wavelengths: on the top, the entire wavelength range is integrated to reproduce the previous result. Left is the contour map for the variation of the static from the smooth case, right is for the variation of the dynamic from the smooth. The white lines are the trace of the peaks; the dotted lines overlapping them are the power-law fits; all levels are the same as in figure 6

However, if the contour plot of the deviation is recalculated according to the above procedure for only small wavelength contributions to $\overline{u'^2}(x, y)$, then the static and dynamic cases appear identical. And since, for the static case, this particular range is assumed to relate to near-wall turbulent motions which were displaced over the two-dimensional roughness, as well as shedding from the elements, it could be inferred that this range also describes similar behavior in the dynamic case. It is observed further that the structures associated with this range move away from the wall at an identical rate between the static and dynamic cases. Whereas, when the contours are recalculated based on contributions from large wavelengths – the kind associated with the dynamic perturbation – the shift of the associated 'hump' away from the wall occurs at vastly different

rates between the two cases.

In some sense, the 'hump' from the dynamic perturbation has been decomposed into a contribution which behaves like the 'hump' from the statically perturbed case, as well as additional energetic content from the dynamic perturbation itself, and these two distinct contributions behave differently both in spatial extent in the flow field, and in the rate at which they evolve downstream.

VI. Conclusions

Comprehensive statistical results for the effect of static and dynamic roughness perturbations were presented, and the 'hump' in the turbulent intensity profile usually associated with roughness effects was shown to behave differently between the two types of perturbations, both in its evolution and spatial extent. Composite spectra provided visual evidence for the destruction of the near wall peak immediately downstream of the perturbations, and its recovery farther downstream. In addition, the spectral signature of the 'hump' was broader (in wavelength) for the static than the dynamic cases. Reconstructing the turbulence intensity through integration of the spectra indicated that the 'hump' in turbulence intensity as a result of the dynamic perturbation contained within it structures associated with the static perturbation, in addition to longer structures associated with the dynamic perturbation, and that these two sets of structures progressed through the boundary layer at different rates.

This work is supported by the Air Force Office of Scientific Research Hypersonics and Turbulence portfolio, under grant #FA9550-08-1-0049 (Program manager John Schmisseur).

References

[1]Hamilton, J., Kim, J., and Waleffe, F., "Regeneration mechanisms of near-wall turbulence structures," *Journal of Fluid Mechanics*, Vol. 287, 1995, pp. 317–348.

[2]Jiménez, J. and Pinelli, A., "The autonomous cycle of near-wall turbulence," *Journal of Fluid Mechanics*, Vol. 389, 1999, pp. 335–359.

[3]Jiménez, J., "Turbulent flows over rough walls," *Annual Review of Fluid Mechanics*, Vol. 36, 2004, pp. 173–196.

[4]Smits, A. and Wood, D., "The response of turbulent boundary layers to sudden perturbations," *Annual Review of Fluid Mechanics*, Vol. 17, 1985, pp. 321–358.

[5]Antonia, R. and Luxton, R., "The response of a turbulent boundary layer to a step change in surface roughness Part 1. Smooth to rough," *J. Fluid Mech*, Vol. 48, No. 4, 1971, pp. 721–761.

[6]Antonia, R. and Luxton, R., "The response of a turbulent boundary layer to a step change in surface roughness Part 2. Rough-to-smooth," *J. Fluid Mech*, Vol. 53, No. 4, 1972, pp. 737–757.

[7]Andreopoulos, J. and Wood, D., "The response of a turbulent boundary layer to a short length of surface roughness," *J. Fluid Mech*, Vol. 118, 1982, pp. 143–164.

[8]Volino, R., Schultz, M., and Flack, K., "Turbulence structure in a boundary layer with two-dimensional roughness," *Journal of Fluid Mechanics*, Vol. 635, 2009, pp. 75–101.

[9]McKeon, B. J., Jacobi, I., and LeHew, J., "Perturbation of a turbulent boundary layer by spatially-impulsive dynamic roughness," *AIAA Paper AIAA 2009-3566*, 2009.

[10]Leonardi, S., Orlandi, P., Smalley, R., Djenidi, L., and Antonia, R., "Direct numerical simulations of turbulent channel flow with transverse square bars on one wall," *Journal of Fluid Mechanics*, Vol. 491, 2003, pp. 229–238.

[11]Antonia, R. and Luxton, R., "The response of a turbulent boundary layer to an upstanding step change in surface roughness," *Journal of Basic Engineering*, Vol. 93, 1971, pp. 22–34.